water

MDPI

Article

Highly Efficient Degradation of Sulfisoxazole by Natural Chalcopyrite-Activated Peroxymonosulfate: Reactive Species and Effects of Water Matrices

Wei Zhou [1,2], Yu Li [1,2], Min Zhang [1,2], Guang-Guo Ying [1,2,*] and Yong Feng [1,2,*]

[1] Guangdong Provincial Key Laboratory of Chemical Pollution and Environmental Safety & MOE Key Laboratory of Theoretical Chemistry of Environment, SCNU Environmental Research Institute, South China Normal University, Guangzhou 510006, China
[2] School of Environment, South China Normal University, University Town, Guangzhou 510006, China
* Correspondence: guangguo.ying@m.scnu.edu.cn (G.-G.Y.); fengy@scnu.edu.cn (Y.F.); Tel.: +86-020-84721549 (Y.F.); Fax: +86-020-85213484 (Y.F.)

Abstract: In this study, chalcopyrite ($CuFeS_2$), a natural mineral with a bimetallic structure, was used as the activator to generate radicals for removing organic pollutants from aqueous solutions via the activation of peroxymonosulfate (PMS). Sulfisoxazole (SIX), a sulfonamide antibiotic, was selected as the model pollutant. The results showed that chalcopyrite was highly reactive toward the activation of PMS; under the conditions of 50 μM PMS and 1 g/L chalcopyrite, approximately 95.7% of the SIX was degraded after reaction for only 5 min. An increase in the loading of chalcopyrite (0.25–2 g/L) promoted the degradation of SIX, while elevated levels of PMS (0.05–0.5 mM) slightly retarded the degradation kinetics. Although the best performance was observed under acidic conditions (pHs 3 and 4), near complete degradation of SIX was also achieved at pH 5.5. Identification of reactive species revealed that both a hydroxyl radical and a sulfate radical were formed in chalcopyrite–PMS oxidation, and they were responsible for the degradation of SIX. Trace amounts of copper and iron were leached out from chalcopyrite during the activation, and both the heterogeneous and homogeneous activation of PMS contributed to the generation of oxidizing radicals. Common water constituents including Cl^-, HCO_3^-, and natural organic matter at their environmentally relevant levels showed a limited effect on the degradation of SIX, which suggests that chalcopyrite–PMS oxidation has high reactivity and stability in the degradation of organic pollutants and shows great practical application potential.

Keywords: peroxymonosulfate; $CuFeS_2$; sulfate radicals; sulfide mineral; water matrices

Citation: Zhou, W.; Li, Y.; Zhang, M.; Ying, G.-G.; Feng, Y. Highly Efficient Degradation of Sulfisoxazole by Natural Chalcopyrite-Activated Peroxymonosulfate: Reactive Species and Effects of Water Matrices. *Water* **2022**, *14*, 3450. https://doi.org/10.3390/w14213450

Academic Editor: Stefano Papirio

Received: 12 October 2022
Accepted: 26 October 2022
Published: 29 October 2022

1. Introduction

Since 1942, when penicillin was first used in clinical treatment, thousands of other antibiotics have been synthesized and adopted to the treatment of human and animal infections. Due to the unsatisfactory removal in wastewater treatment plants [1] and unregulated discharge of household and livestock effluents [2], huge amounts of antibiotics are released into the environment [3–5]. The ubiquitous presence of antibiotics in the environment greatly stimulates the emergence of antibiotic-resistant bacteria (ARB) and antibiotic resistant genes (ARGs) [6,7], which reduces the therapeutic potential of antibiotics against human and animal pathogens. A recent study estimates that approximately 1.27 million deaths are attributable to bacterial antimicrobial resistance [8]. Therefore, efficient treatment technologies to remove antibiotics from aqueous solutions are urgently required.

Among the water and wastewater treatment technologies, the advanced oxidation processes relying on powerful oxidizing radicals, such as sulfate radicals ($SO_4^{\cdot-}$,

$E^0(SO_4^{\cdot-}/SO_4^{2-}) = 2.5 - 3.1$ V) and hydroxyl radicals (·OH, $E^0(\cdot OH/OH^-) = 1.8 - 2.7$ V) [9], have increasingly attracted attention for antibiotic removal [10–12]. Of the various advanced oxidative systems, the activation of persulfates including peroxymonosulfate (PMS) and peroxydisulfate (PDS) is of great interest to environmental scientists because these peroxides could form both $SO_4^{\cdot-}$ and ·OH simultaneously and can be easily activated by a wide range of functional materials, such as naturally occurring minerals [13,14], transition metals-based nanocomposites [15–18], and carbonaceous materials [19–24]. Compared with the latter two kinds of activators, naturally occurring minerals are more promising for practical applications because they are cheap, easily available, and have stable catalytic reactivity. For example, pyrite, the most abundant sulfur mineral on earth, can activate both PMS and PDS to form highly oxidizing radicals and does not deactivate in successive catalytic cycles [25–28]. Mechanism investigation showed that the low-valent state of sulfur in pyrite promoted the circulation of activate sites (e.g., Fe(III)/Fe(II)) during the activation of persulfates by pyrite [28,29]. In addition, a synergistic catalytic effect is expected to form and improve the activation and degradation when some bimetallic minerals (oxides) are used as the activator [30–32]. Therefore, natural minerals with multiple active sites have great advantages for the generation of radicals.

In this study, naturally occurring chalcopyrite ($CuFeS_2$) was used to remove sulfisoxazole, a representative antibiotic, via the activation of PMS. Sulfisoxazole is a commonly used sulfonamide antibiotic and has been frequently detected in the environment [33,34]. Chalcopyrite is cost-effective for environmental remediation with easy availability because it is the most abundant component in the sulfide copper-bearing deposits [35]. In addition, chalcopyrite contains Cu(I) and Fe(III); the potential synergy between these two elements were expected to facilitate the activation of PMS. To reveal the catalytic reactivity of chalcopyrite, the degradation of SIX in the presence of different activators was investigated and compared and several potential influencing parameters were studied. The primary reactive species were studied by electron paramagnetic resonance and scavenging experiments. To reveal the stability and tolerance of chalcopyrite–PMS oxidation, the impacts of common anions and natural organic matter (NOM) were investigated.

2. Experimental

2.1. Materials

Oxone ($KHSO_5 \cdot 1/2KHSO_4 \cdot 1/2K_2SO_4$), the commercial form of PMS, was obtained from Sigma-Aldrich (St. Louis, MO, USA). Raw chalcopyrite was collected from a copper mine in Guizhou Province, China and was crushed by ball mill (JX-4G, Jingxin, Shanghai, China) before use. In addition to the main composition chalcopyrite ($CuFeS_2$, PDF #37-0471), the mineral sample also contained calcium silicate hydrate (PDF #33-0306) as the primary impurity (Figures S1 and S2 in Supplementary Material). Sulfisoxazole (SIX, 99%), nanoscale magnetite (Fe_3O_4), standard solutions of iron (1000 mg/L) and copper (1000 mg/L) for ICP-MS, potassium iodide (98%), furfuryl alcohol (98%), sodium thiosulfate (99%), and *tert*-butanol (TBA; ACS) were obtained from Aladdin Corporation (Shanghai, China). The particle size of the nano magnetite was generally in the range of 10 to 30 nm (Figure S3). HPLC-grade methanol (MeOH) was purchased from the ANPEL Laboratory (Shanghai, China). The ultrapure water with a resistivity of greater than 18.2 MΩ cm was prepared with a Millipore IQ 7010 water purification system (Burlington, MA, USA). Suwannee River NOM was obtained from IHSS (Denver, CO, USA).

2.2. Degradation Experiments

The adsorption and catalytic degradation experiments were performed in 200 mL GG-17 glass reactors (Sichuan Shubo Co. LTD, Chengdu, Sichuan Province, China) at room temperature (23 ± 2 °C) in the presence of air. Typically, 95 mL of deionized water was added to the glass reactor, followed by the addition of PMS. As the dissolution of PMS acidified the solution, its pH value was adjusted to the desired value (3, 4, 5.5, or 7)

using 0.1 M sulfuric acid or sodium hydroxide. A quantity of 5 mL of the SIX stock solution (100 mg/L) was then transferred to the PMS solution to achieve an initial concentration of 5 mg/L, and chalcopyrite was added immediately to the SIX–PMS solution to initiate catalytic degradation. In the scavenging experiments, alcohol scavengers were added before the introduction of chalcopyrite. To maintain the suspension of solids, the reaction was agitated on a RO5 magnetic stirrer (IKA Works, Guangzhou, Guangdong Province, China) at a rotation speed of 400 rpm. The reaction lasted for 30 min, and aqueous samples were withdrawn using 1 mL syringes (ANPEL Laboratory, Shanghai, China) at certain intervals, filtered with 0.22 μm polytetrafluoroethylene membrane filters (ANPEL Laboratory, Shanghai, China), quenched by thiosulfate, and stored in LC vials for HPLC analysis.

To investigate the reutilization performance of chalcopyrite, the degradation of SIX by chalcopyrite–PMS oxidation was evaluated in successive activation cycles. After each cycle, the solids were recollected by vacuum filtration and washed three times with deionized water. The next cycle was initiated by transferring the cleaned solids to the SIX–PMS solution.

2.3. Material Characterization

A D8 Advance X-ray diffractometer (Bruker Corporation, Karlsruhe , Germany) was used to study the purity and composition of chalcopyrite. A Kratos AXIS Supra X-ray photoelectron spectrometer (AXIS Supra, Manchester, UK) was employed to examine the surface chemical states of chalcopyrite. A Micromeritics ASAP 2020 surface area analyzer (Micromeritics, GA, USA) was used to determine the Brunauer–Emmett–Teller (BET) specific surface area of solid materials. A JEOL JES FA200 electron paramagnetic resonance (EPR) spectrometer (JEOL Ltd., Tokyo, Japan) was employed to investigate oxygen-containing radicals. A TESCAN CLARA scanning electron microscope (SEM) (TESCAN, Brno, Czech Republic) was used to explore the morphology of chalcopyrite.

2.4. Chemical Analysis

The concentration of SIX was measured using HPLC (Agilent 1260 Infinity II) coupled with a diode array detector (Agilent, Santa Clara, CA, USA) and a Poroshell 120 EC-C18 column (100 mm × 2.1 mm, 2.7 μm) (Agilent, Santa Clara, CA, USA). Ultrapure water and HPLC-grade MeOH (40:60, *v*/*v*%) were used as the mobile phase at a flow rate of 1 mL/min. The iron and copper leached from chalcopyrite were detected using ICP-MS (Agilent 7900). The concentration of PMS was determined spectrophotometrically at 352 nm by the iodometric method [36]. Total organic carbon (TOC) was measured using a Shimadzu TOC analyzer (Shimadzu, Kyoto, Japan). The degradation products of SIX were monitored using LC-MS/MS (Waters, Milford, MA, USA), details of which are documented in Note S1. The pH value was measured using a Thermo Scientific pH meter (Orion™ Versa Star, Waltham, MA, USA).

3. Results and Discussion

3.1. Degradation of SIX by Chalcopyrite–PMS Oxidation

The reactivity of chalcopyrite toward PMS activation was evaluated by comparing the degradation of SIX under different reaction conditions. As shown in Figure 1a, no obvious removal of SIX was noticed when chalcopyrite was present alone, which suggests that this mineral had limited adsorption capacity for SIX. This result is consistent with the low specific surface area and absence of pores on the surface of chalcopyrite (Figure S2). When PMS was present alone, approximately 35.2% of the SIX was removed, which could be related to the direct oxidation by PMS [37,38]. According to Yin et al. [1], such oxidation most likely occurred through the adduction on the N atom adjacent to the benzene ring of SIX to form a nitroso or nitro group. When PMS was co-present with chalcopyrite, rapid acceleration in the degradation of SIX was observed; approximately 99.3% of the SIX was

removed after 15 min. These observations reveal that chalcopyrite had great capability in the activation of PMS for SIX degradation. The reutilization ability of chalcopyrite was evaluated by exploring the degradation of SIX in consecutive activation cycles. As shown in Figure S4, approximately 100%, 94.9%, 80%, 81%, and 72.1% of the SIX was removed in the 1st, 2nd, 3rd, 4th, and 5th activation cycles, respectively. No new substance (s) was formed on the surface of chalcopyrite after the reaction (Figure S5). These observations suggest that chalcopyrite could be reused. In addition, approximately 25% of the TOC was removed after 30 min (Figure S6), demonstrating that chalcopyrite–PMS oxidation had the capability of mineralizing SIX to carbon dioxide and water.

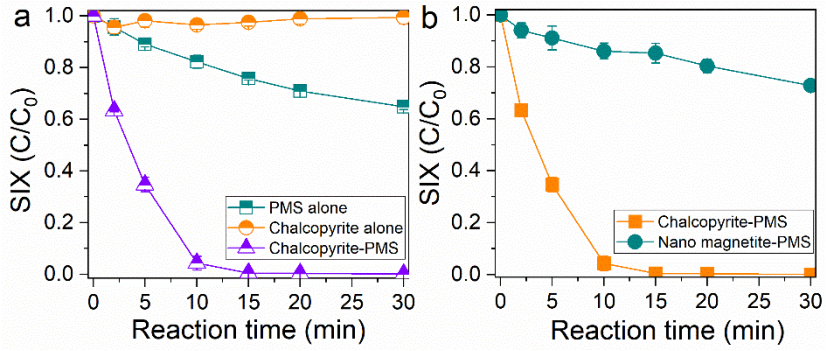

Figure 1. (**a**) Degradation of SIX by chalcopyrite–PMS oxidation and (**b**) reactivity of different activators. Conditions: [SIX] = 5 mg/L, [PMS] = 0.5 mM, [chalcopyrite] = [magnetite] = 1 g/L, and pH 3.0.

To further demonstrate the reactivity of chalcopyrite, the degradation of SIX by nano magnetite–PMS was investigated and compared. As shown in Figure 1b, only approximately 26.9% of the SIX was degraded by nano magnetite–PMS oxidation and this degradation rate was significantly lower than that achieved by chalcopyrite–PMS oxidation. Kinetic investigation showed that the degradation of SIX in the first 15 min followed the pseudo-first-order kinetics (Figure S7). Through calculation, the rate constants for SIX degradation by chalcopyrite–PMS oxidation and nano magnetite–PMS oxidation were 0.314 and 0.014 min^{-1}, respectively. The former rate constant was 22 times greater than the latter one. These results demonstrate that chalcopyrite had high reactivity for SIX degradation by activating PMS.

3.2. Effects of Influencing Factors

To comprehensively investigate the reactivity of chalcopyrite–PMS oxidation, the effects of potential influencing factors including PMS doses, chalcopyrite loadings, and solution pH values were explored. Under the conditions of 0.05 mM PMS, 1 g/L chalcopyrite, and pH 3.0, approximately 97.3% of the SIX was degraded after 10 min. Meanwhile, the removal kinetics of SIX decreased slightly when PMS was enhanced from 0.05 to 0.5 mM (Figure 2a), which could most likely be related to the scavenging role of excess PMS (Equation (1)) [39]. A similar phenomenon was also observation by Peng et al. [40].

$$HSO_5^- + SO_5^{\cdot -} \rightarrow SO_4^{2-} + SO_5^{\cdot -} + H^+ \quad (1)$$

When the concentration of chalcopyrite ranged from 0.25 to 2 g/L, an increase in the loading accelerated the degradation of SIX (Figure 2b), and the degradation kinetics were positively correlated with the loading of chalcopyrite. For example, the degradation rate of SIX was increased from 51.9% to 99.6% in the presence of 0.25 and 1 g/L chalcopyrite, respectively, after 15 min. As the removal of SIX was mainly due to the activation of PMS, the promotion effect of chalcopyrite could be ascribed to the increase in the number of activation sites.

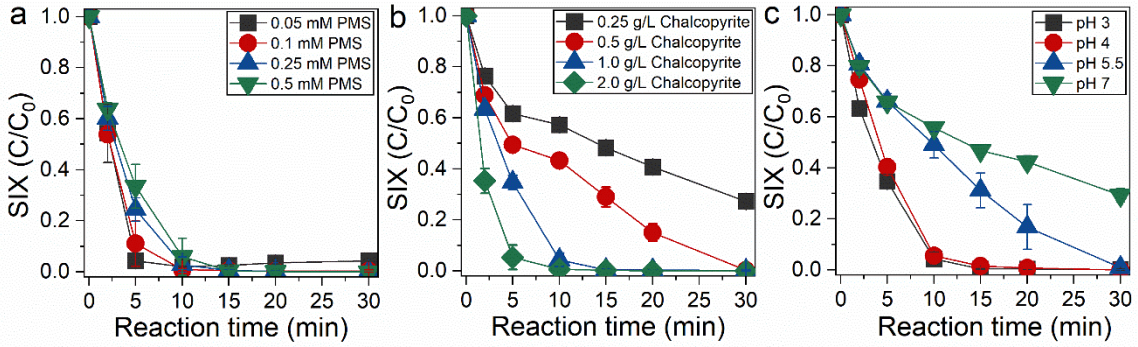

Figure 2. Effects of (**a**) PMS, (**b**) chalcopyrite, and (**c**) solution pH values on the degradation of SIX by chalcopyrite–PMS oxidation. Conditions: [SIX] = 5 mg/L, (**b**,**c**) [PMS] = 0.5 mM, (**a**,**c**) [chalcopyrite] = 1 g/L, and (**a**,**b**) pH 3.0.

The pH value of real wastewater ranges widely, and therefore, the influence of solution pH value on the degradation of SIX by chalcopyrite–PMS was explored. As shown in Figure 2c, the removal of SIX did not vary notably when the pH value was increased from 3 to 4. Although a further increase in the pH value to 5.5 slowed down the degradation kinetics, an identical overall degradation rate of approximately 99.1% was achieved. When the pH value was enhanced to 7, a pronounced decrease in the removal of SIX was observed. The isoelectric point of chalcopyrite was measured to be lower than 4.0 [40], which suggests that chalcopyrite was negatively charged when the pH value ranged from 4.0 to 7.0 and the amount of negative charge was increased with the enhancement of the pH value. Meanwhile, the pK_{a1} and pK_{a2} of SIX are 1.5 and 5.0 [41], respectively, which suggests that SIX mainly existed in a dissociated form at elevated pH values (pHs 5.5 and 7.0) and was negatively charged. There was electrostatic repulsion between dissociated SIX and chalcopyrite at pHs 5.5 and 7.0, and a stronger repulsion effect was expected with a higher pH value, which explains the decrease in the degradation kinetics of SIX at pHs 5.5 and 7.0. A similar effect of electrostatic force in the degradation of SIX was also reported by Wang et al. [42]. Meanwhile, the speciation and dissolution of metal ions leached from chalcopyrite were expected to be affected by the pH value, which might also influence the degradation of SIX. In addition, the speciation and oxidizing capability of radicals changed as the pH value was increased from 3 to 7 [2,3], which might also influence the degradation.

3.3. Reactive Species and Activation Mechanisms

Reactive species, such as ·OH and $SO_4^{\cdot-}$, were expected to form during the activation of PMS by chalcopyrite. To clarify this, the EPR spectrum of chalcopyrite–PMS oxidation was investigated. As shown in Figure 3a,b, four-fold characteristic peaks (1:2:2:1) were successfully recorded, and the intensity of these peaks increased with the extension of the activation reaction. These peaks were indexed to the signal of DMPO–·OH adducts, revealing that ·OH was generated in chalcopyrite–PMS oxidation. Moreover, the adducts of DMPO–$SO_4^{\cdot-}$ were recorded, which demonstrates that $SO_4^{\cdot-}$ was also produced. As $SO_4^{\cdot-}$ was present, it is worth mentioning that the ·OH could be formed by either the activation of PMS or the transformation of $SO_4^{\cdot-}$. It was reported that the spin adducts of $SO_4^{\cdot-}$ (DMPO–$SO_4^{\cdot-}$) could decay to that of ·OH (DMPO–·OH) via nucleophilic substitution [43,44] and $SO_4^{\cdot-}$ could transform to ·OH by reacting with H_2O (≤5×10^2 s^{-1}) [45] or OH^- (4.6×10^7 M^{-1} s^{-1}) [46].

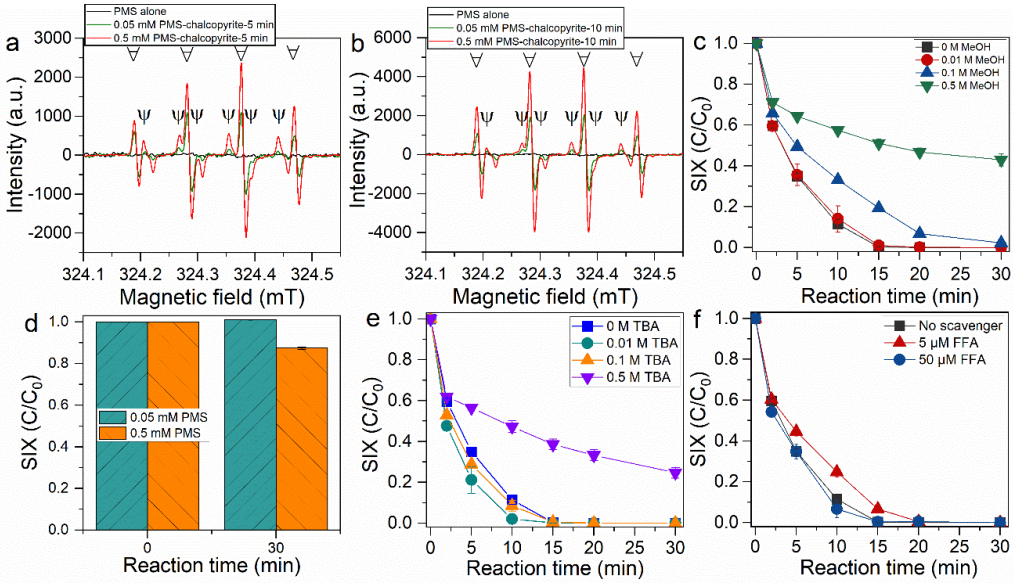

Figure 3. EPR spectra of chalcopyrite–PMS oxidation after reaction for (**a**) 5 and (**b**) 10 min; effects of (**c**,**d**) MeOH, (**e**) TBA, and (**f**) FFA on the degradation of SIX by chalcopyrite–PMS oxidation. Conditions: [SIX] = 5 mg/L, (**c**–**f**) [PMS] = 0.5 mM, [chalcopyrite] = 1 g/L, (**d**) [MeOH] = 5 M, and pH 3.0.

Although both $SO_4^{\cdot-}$ and ·OH were most likely formed in chalcopyrite–PMS oxidation, their role in the degradation of SIX was still unclear. To reveal the contribution of these reactive species, classical scavenging experiments via testing the effects of different alcohols (MeOH and TBA) were performed. MeOH that contains an α-H interacts rapidly with both $SO_4^{\cdot-}$ (1.0×10^7 M^{-1} s^{-1}) [47] and ·OH (9.7×10^8 M^{-1} s^{-1}) [48], while TBA without an α-H has highly reactivity only toward ·OH (6.0×10^8 M^{-1} s^{-1}) [48] and reacts with $SO_4^{\cdot-}$ (4.0×10^5 M^{-1} s^{-1}) [49] quite slowly. As shown in Figure 3c, the presence of MeOH significantly inhibited the degradation of SIX and the inhibitory effect was positively correlated with the concentration of MeOH. When the concentration of MeOH was increased to 5 M, the overall degradation rates of SIX were decreased to 0% and 12.5% in the presence of 0.05 and 0.5 M PMS (Figure 3d), respectively. As observed in Figure 1a, the slight degradation of SIX in the presence of 0.5 M PMS could be related to its oxidation by PMS. The almost complete inhibition on the degradation of SIX by MeOH suggests that radicals were the key oxidizing species. Meanwhile, TBA with a same concentration had a much smaller inhibitory effect than MeOH (Figure 3e). For example, the pseudo-first-order rate constants for the degradation of SIX in the presence of 0 M scavenger, 0.1 M MeOH, and 0.1 M TBA were 0.214, 0.104, and 0.243 min^{-1} (Figure S8), respectively. As the rate constants of ·OH with MeOH and TBA are at the same order of magnitude (~10^8 M^{-1} s^{-1}), the relatively less efficient scavenging performance of TBA was most likely due to the involvement of $SO_4^{\cdot-}$ during the degradation of SIX by chalcopyrite–PMS oxidation.

In addition to radicals, singlet oxygen ($^1O_2$) [16,50] and high-valent metal species, such as iron–oxo species and Cu^{3+} [51–53], have been proposed to be the reactive species during the activation of PMS (PDS) by some transition metals-based materials. In this study, the potential contribution of $^1O_2$ was explored by investigating the effect of furfuryl alcohol (FFA) on the degradation of SIX. FFA is a commonly used scavenger of $^1O_2$ (1.2×10^8 M^{-1} s^{-1}) [54]. The quenching test showed that FFA with a concentration of 5 or 50 μM had no obvious influence on the degradation of SIX by chalcopyrite–PMS oxidation (Figure 3f), which suggests that $^1O_2$ contributed negligibly to the degradation of SIX. Meanwhile, the possible involvement of Cu^{3+} was explored by investigating the UV–Vis adsorption spectrum of chalcopyrite–PMS oxidation. It has been reported that Cu^{3+} forms a complex with periodate in water solutions, and this complex has a characteristic absorption

peak at approximately 425 nm (Figure 4a) [55,56]. However, no such absorbance was observed at 425 nm in the UV–Vis spectra of chalcopyrite–PMS oxidation, suggesting that no Cu^{3+} was generated during the activation of PMS by chalcopyrite. During the activation of PMS, metal ions were expected to leach out from the surface of chalcopyrite. Therefore, the dissolved metals were quantified. As shown in Figure 4b, both dissolved copper (Cu^{2+}, Cu^{+}) and iron (Fe^{3+}, Fe^{2+}) were detected, and they were noticed to accumulate with the continuation of the catalytic reaction. After reaction for 30 min, the total dissolved copper and iron were measured to be 1.62 and 0.43 mg/L, respectively. Meanwhile, the XPS results show that the atomic ratio between copper and iron on the surface of chalcopyrite was decreased from 1.02 to 0.42 after the catalytic reaction. These results suggest that the dissolution of copper from the surface of chalcopyrite was more rapid than that of iron. This conclusion is in line with previous studies on the use of copper–iron bimetallic oxides for PMS activation [30,57]. Meanwhile, the reduction states of copper (Cu^{+}) and iron (Fe^{2+}) were detected, and they were generally observed to accumulate during the interaction of chalcopyrite with PMS, suggesting that there were redox cycles involving both Cu^{2+} (≡Cu(II)) and Fe^{3+} (≡Fe(III)). Although Cu^{2+} and Fe^{3+} were less efficient for the activation of PMS (Figure S9), reactive species were expected to be formed via the interaction of Cu^{+} with dissolved molecular oxygen (or PMS) [58,59] and the interaction of Fe^{2+} with PMS [26].

To reveal the activation mechanism of PMS and the activation sites, the XPS spectra of chalcopyrite were recorded. The XPS survey spectra showed that the ratio between Cu and Fe on the surface of chalcopyrite decreased from 1.01 to 0.42 after the activation reaction (Figure 5a and Table S1). Meanwhile, the ratio between Fe and S increased from 0.45 to 0.83. These results revealed that, during the activation, the leaching of Cu and S from the surface of chalcopyrite was more rapid than that of Fe, which is consistent with the dissolved metal analysis (Figure 4b). Meanwhile, the high-resolution (Figure 5b) Fe $2p_{3/2}$ and (Figure 5c) Cu $2p_{3/2}$ XPS spectra showed that the ratio of metals at different valent states was changed after the reaction, indicating that there were redox reactions on the surface of chalcopyrite during the activation. The high-resolution S 2p XPS spectrum showed that the S on the surface of chalcopyrite existed at different states including S^{2-}, S_2^{2-}, and S_n^{2-}. After the activation reaction, the content of S_n^{2-} decreased while the percentages of both S^{2-} and S_2^{2-} increased, suggesting that there were transformation reactions among these S species during the activation of PMS. Similar observations were also reported by Wang et al. [60]. On the basis of these discussions, a tentative mechanism was proposed for the activation of PMS and catalytic degradation of SIX. The mechanism includes three stages (radical generation, activator regeneration, and SIX degradation). First, Cu^{+} reacted with dissolved oxygen to generate ·OH (Equations (2)–(4)), and meanwhile, Cu^{+} and Fe^{2+} and their solid forms interacted with PMS to produce $SO_4^{\cdot-}$ (Equations (5)–(8)). During the reaction, the activators themselves were oxidized. Second, $SO_4^{\cdot-}$ transformed to ·OH via reaction with H_2O and OH^- (Equation (9)). Third, Cu^{+} and surface S species (≡S^{2-}, ≡ S_2^{2-}, and ≡ S_n^{2-}) are reductants and transformed the oxidized forms of activators back to their reduction states (Equations (10)–(14)). Finally, the generated $SO_4^{\cdot-}$ and ·OH interacted with SIX and degraded this contaminant (Equation (15)). It is worth mentioning that the direct oxidation of SIX by PMS also contributed to the degradation, although this mechanism was relatively much less important.

$$Cu^{+} + O_2 \rightarrow Cu^{2+} + O_2^{\cdot-} \quad (2)$$

$$Cu^{+} + O_2^{\cdot-} + 2H^{+} \rightarrow Cu^{2+} + H_2O_2 \quad (3)$$

$$Cu^{+} + H_2O_2 \rightarrow Cu^{2+} + \cdot OH + OH^{-} \quad (4)$$

$$Cu^{+} + HSO_5^{-} \rightarrow Cu^{2+} + SO_4^{\cdot-} + OH^{-} \quad (5)$$

$$Fe^{2+} + HSO_5^{-} \rightarrow Fe^{3+} + SO_4^{\cdot-} + OH^{-} \quad (6)$$

$$\equiv Cu(I) + HSO_5^- \rightarrow \equiv Cu(II) + SO_4^{\cdot -} \quad (7)$$

$$\equiv Fe(II) + HSO_5^- \rightarrow \equiv Fe(III) + SO_4^{\cdot -} \quad (8)$$

$$SO_4^{\cdot -} + OH^-/H_2O \rightarrow \cdot OH \quad (9)$$

$$Cu^+ + Fe^{3+} \rightarrow Cu^{2+} + Fe^{2+} \quad (10)$$

$$Cu^+ + \equiv Fe(III) \rightarrow \equiv Fe(II) + Cu^{2+} \quad (11)$$

$$\equiv Cu(I) + Fe^{3+} \rightarrow \equiv Cu(II) + Fe^{2+} \quad (12)$$

$$\equiv S^{2-}(\equiv S_2^{2-}, \equiv S_n^{2-}) + Cu^{2+}(Fe^{3+}) \rightarrow Cu^+(Fe^{2+}) + \text{sulphur} - \text{containing anions} \quad (13)$$

$$\equiv S^{2-}(\equiv S_2^{2-}, \equiv S_n^{2-}) + \equiv Cu^{2+}(\equiv Fe^{3+}) \rightarrow \equiv Cu^+(\equiv Fe^{2+}) + \text{sulphur} - \text{containing anions} \quad (14)$$

$$SO_4^{\cdot -}/\cdot OH + SIX \rightarrow \text{degradation products} \quad (15)$$

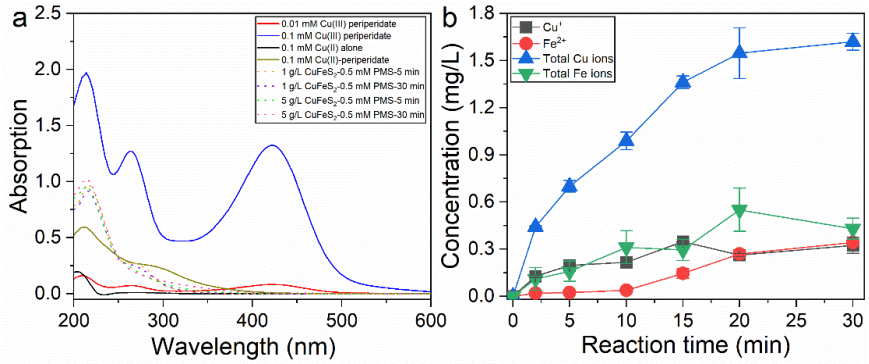

Figure 4. (**a**) UV–Vis adsorption spectra of different reaction systems; (**b**) concentrations of dissolved iron and copper ions in chalcopyrite–PMS oxidation. The difference between the concentrations of total dissolved copper (iron) ions and Cu^+ ions (Fe^{2+}) represents Cu^{2+} (Fe^{3+}).

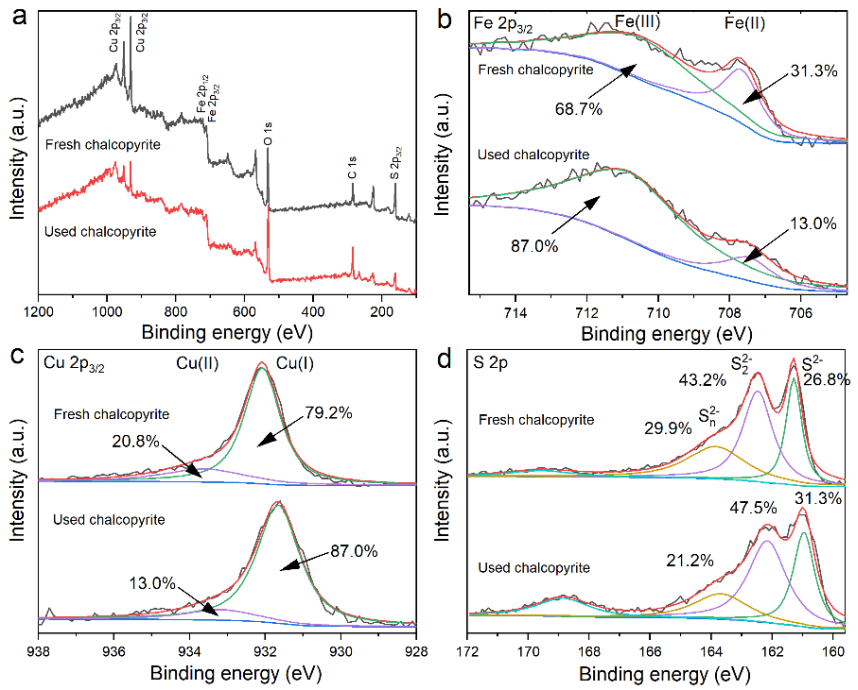

Figure 5. XPS spectra of fresh and used chalcopyrite: (**a**) survey spectra, (**b**) Fe 2p3/2, (**c**) Cu 2p3/2, and (**d**) S 2p.

To reveal the fate and degradation pathways of SIX (Figure S10), its degradation products were investigated using LC-MS/MS. As listed in Table S2, four intermediates including TP1 (Figure S11), TP2 (Figure S12), TP3 (Figure S13), and TP4 (Figure S14) were detected. On the basis of these intermediates, we proposed that SIX was most likely degraded in two different pathways (Figure S15). In pathway 1, TP1 with an *m*/*z* of 156 was formed, which could be ascribed to the cleavage of the S–N bond in SIX. In the presence of ·OH, electrophilic addition occurred and generated TP2 (*m*/*z* 192). In pathway 2, the C–N bond in SIX cleaved under the attack of radicals, generating TP3 (*m*/*z* 173) as one of the major products. ·OH was then reacted with TP3 to produce an intermediate with an *m*/*z* of 189, which combined subsequently with the substance generated during the cleavage of the S–N bond to form TP4 (*m*/*z* 297). Under the further attack of both ·OH and $SO_4^{\cdot-}$, these products were degraded to small-molecular organic acids and even mineralized.

3.4. Effects of Common Water Components

To evaluate the practical application potential of chalcopyrite–PMS oxidation, the impacts of common water constituents including Cl^-, HCO_3^-, and NOM on the degradation of SIX were investigated. Cl^- with a concentration in the range of 0.5 to 5 mM did not have an obvious effect on chalcopyrite–PMS oxidation (Figure 6a). When its concentration was further enhanced to 10 mM, a slight inhibitory impact on the degradation kinetics was noticed. This impact could be related to the scavenging roles of excess Cl^- toward $SO_4^{\cdot-}$ ($k = 3.1 \times 10^8$ M^{-1} s^{-1}) [46], ·OH ($k = 4.3 \times 10^9$ M^{-1} s^{-1}) [61], and PMS ($k = (2.06 \pm 0.03) \times 10^{-3}$ M^{-1} s^{-1}) [62]. In these reactions, the radicals and PMS were transformed to chlorine-reactive species. The reactions of excess Cl^- with radicals generated $Cl_2^{\cdot-}$, which is a reactive species with a much lower redox potential ($E^0(Cl_2^{\cdot-}/2Cl^-) = 2.09$ V) [9]. Meanwhile, the interaction between Cl^- and PMS produced HOCl and Cl_2. These chlorine-containing species are less reactive than both $SO_4^{\cdot-}$ and ·OH.

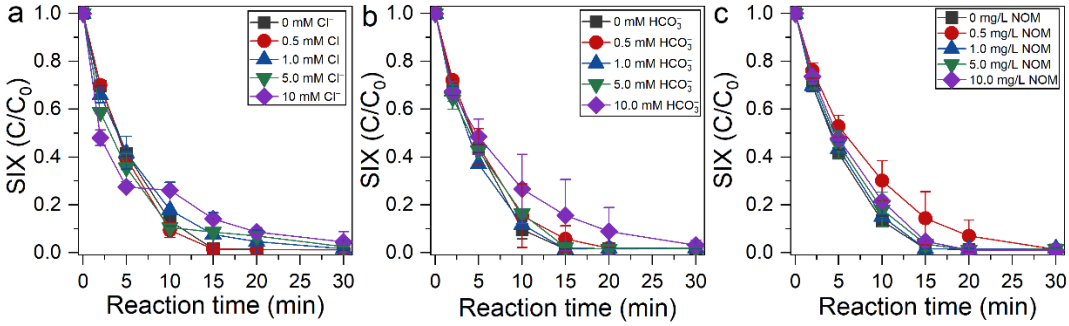

Figure 6. Effects of (**a**) Cl^-, (**b**) HCO_3^-, and (**c**) NOM on the degradation of SIX by chalcopyrite–PMS oxidation.

In analogy to the case of Cl^-, HCO_3^- (0.5–5 mM) had no obvious effect on the degradation of SIX and a slight retarding effect was observed when the level of HCO_3^- was increased to 10 mM (Figure 6b). Like Cl^-, HCO_3^- is also a radical scavenger and reacts with either $SO_4^{\cdot-}$ ($(9.1 \pm 0.4) \times 10^6$ M^{-1} s^{-1}) [46] or ·OH (8.5×10^6 M^{-1} s^{-1}) [63] to generate carbonate radicals ($CO_3^{\cdot-}$). The generated $CO_3^{\cdot-}$ ($E^0(CO_3^{\cdot-}/CO_3^{2-}) = 1.65$ V) is much less oxidizing than both $SO_4^{\cdot-}$ and ·OH, which could explain the inhibitory effect of HCO_3^-. In addition, the buffer effect of HCO_3^- might also influence the degradation of SIX.

The investigation on the NOM showed that this substance with a concentration of 0.5 mg/L slightly slowed down the degradation of SIX (Figure 6c), which could be explained by the scavenging effect of NOM toward both $SO_4^{\cdot-}$ ($(0.64–3.68) \times 10^7$ M^{-1} s^{-1}) and ·OH (~10^8 M^{-1} s^{-1}) [64]. However, a further increase in the concentration of NOM from 1.0–10.0 mg/L slightly promoted the degradation. This observation could most likely be related to the oxidation of SIX by the reactive species formed during the reaction of PMS with NOM and the accelerated circulation of catalytic sites (e.g., ≡Fe(II) and ≡Cu(I)) by NOM that is

known to be redox reactive [65,66]. It has been reported that quinone groups could activate PMS to form $^1O_2$ [67] and quinone or quinone-like groups are typically present in the structure of NOMs. Overall, the presence of NOM (0–10 mg/L) had no obvious inhibitory effect on chalcopyrite–PMS oxidation, which suggests that this oxidation has high stability and tolerance in the removal of organic contaminant.

4. Conclusions

In this study, a heterogeneous activator of using recycled natural mineral chalcopyrite was used for the degradation of SIX via the activation of PMS. Chalcopyrite–PMS oxidation had high reactivity for SIX degradation and a wide effective pH range. Near complete degradation of SIX was achieved at pH 3.0–5.5. Radicals including $SO_4^{\cdot-}$ and ·OH were generated during the activation of PMS by chalcopyrite and were the key to the degradation of SIX. $^1O_2$ and high-valent metal species were not involved during the degradation of SIX. Traces of metals were leached out from the surface of chalcopyrite during the activation and activated PMS to generate highly oxidizing radicals. Both homogeneous and heterogeneous activation of PMS contributed to the degradation of SIX. Under the attack of radicals, four degradation products were identified. Cl^-, HCO_3^-, and NOM showed limited scavenging effects on the degradation of SIX, demonstrating the great potential of chalcopyrite–PMS oxidation for practical remediation application.

Supplementary Materials: The following supporting information can be downloaded at: https://www.mdpi.com/article/10.3390/w14213450/s1, Note S1: Analysis of degradation products; Table S1: Elemental compositions of fresh and used chalcopyrite; Table S2: Intermediate products of SIX degradation in chalcopyrite-PMS oxidation; Figure S1: Elemental compositions of fresh and used chalcopyrite; Figure S2: (a, b) SEM images of chalcopyrite with different magnifications and (c) EDS spectrum of chalcopyrite; Figure S2: (a, b) SEM images of chalcopyrite with different magnifications and (c) EDS spectrum of chalcopyrite; Figure S3: SEM images of magnetite with different magnifications; Figure S4: Degradation of SIX by chalcopyrite-PMS oxidation in consecutive catalytic cycles.; Figure S5: XRD patterns of fresh and used chalcopyrite; Figure S6: Removal of TOC by chalcopyrite-PMS oxidation; Figure S7: Plot of -ln(C/C0) versus reaction time. The straight line represents linear fitting; Figure S8: Plot of -ln(C/C0) versus reaction time. The straight line represents linear fitting; Figure S9: Degradation of SIX by PMS in the presence of Cu2+ or both Cu2+ and Fe3+.; Figure S10: Fragmentation pattern of SIX; Figure S11: Fragmentation pattern of TP1; Figure S12: Fragmentation pattern of TP2; Figure S13: Fragmentation pattern of TP3; Figure S14: Fragmentation pattern of TP4; Figure S15: Proposed pathways for the degradation of SIX in chalcopyrite-PMS oxidation.

Author Contributions: Conceptualization, Y.F.; methodology, Y.F.; investigation, W.Z. and Y.L.; resources, G.-G.Y., Y.F.; data curation, W. Zhou, M. Zhang; writing—original draft preparation, Y.F.; writing—review and editing, Y.F.; supervision, G.-G.Y., Y.F.; project administration, Y.F.; funding acquisition, M.Z., G.-G.Y., Y.F.. All authors have read and agreed to the published version of the manuscript.

Funding: This work was supported by the National Natural Science Foundation of China (No. 42077340 and No. 52000080) and Guangdong Basic and Applied Basic Research Foundation (No. 2019A1515110988 and No. 2019A1515110131).

Data Availability Statement: Not applicable.

Acknowledgments: The authors gratefully acknowledge the support of 2022 Guangdong-Hong Kong-Macao Greater Bay Area Exchange Programs of SCNU.

Conflicts of Interest: The authors declare no conflict of interest.

Reference

1. Wang, K.; Zhuang, T.; Su, Z.; Chi, M.; Wang, H. Antibiotic residues in wastewaters from sewage treatment plants and pharmaceutical industries: Occurrence, removal and environmental impacts. *Sci. Total Environ.* **2021**, *788*, 147811.
2. Junaid, M.; Zainab, S.M.; Xu, N.; Sadaf, M.; Malik, R.N.; Wang, J. Antibiotics and antibiotic resistant genes in urban aquifers. *Curr. Opin. Environ. Sci. Health* **2022**, *26*, 100324.
3. Zhang, Q.-Q.; Ying, G.-G.; Pan, C.-G.; Liu, Y.-S.; Zhao, J.-L. Comprehensive evaluation of antibiotics emission and fate in the river basins of China: Source analysis, multimedia modeling, and linkage to bacterial resistance. *Environ. Sci. Technol.* **2015**, *49*, 6772–6782.
4. Li, Z.; Li, M.; Zhang, Z.; Li, P.; Zang, Y.; Liu, X. Antibiotics in aquatic environments of China: A review and meta-analysis. *Ecotoxicol. Environ. Saf.* **2020**, *199*, 110668.
5. Basheer, A.A. Chemical chiral pollution: Impact on the society and science and need of the regulations in the 21st century. *Chirality* **2018**, *30*, 402–406.
6. Qiao, M.; Ying, G.-G.; Singer, A.; Zhu, Y.-G. Review of antibiotic resistance in China and its environment. *Environ. Int.* **2018**, *110*, 160–172.
7. Zhu, Y.-G.; Zhao, Y.; Li, B.; Huang, C.-L.; Zhang, S.-Y.; Si-Yu, Z.; Chen, Y.-S.; Zhang, T.; Gillings, M.; Su, J.-Q. Continental-scale pollution of estuaries with antibiotic resistance genes. *Nat. Microbiol.* **2017**, *2*, 16270.
8. Murray, C.J.; Ikuta, K.S.; Sharara, F.; Swetschinski, L.; Aguilar, G.R.; Gray, A.; Han, C.; Bisignano, C.; Rao, P.; Wool, E.; et al. Global burden of bacterial antimicrobial resistance in 2019: A systematic analysis. *Lancet* **2022**, *399*, 629–655.
9. Neta, P.; Huie, R.E.; Ross, A.B. Rate Constants for Reactions of Inorganic Radicals in Aqueous Solution. *J. Phys. Chem. Ref. Data* **1988**, *17*, 1027–1284.
10. Wang, J.; Zhuan, R. Degradation of antibiotics by advanced oxidation processes: An overview. *Sci. Total Environ.* **2020**, *701*, 135023.
11. Qiu, Z.; Xiao, X.; Yu, W.; Zhu, X.; Chu, C.; Chen, B. Selective separation catalysis membrane for highly eficient water and soil decontamination via a persulfate-based advanced oxidation process. *Environ. Sci. Technol.* **2022**, *56*, 3234–3244.
12. Silva, B.S.; Ribeiro, M.C.B.; Ramos, B.; Peixoto, A.L.d. Removal of amoxicillin from processing wastewater by ozonation and UV-aided ozonation: Kinetic and economic comparative study. *Water* **2022**, *14*, 3198.
13. Lai, L.; He, Y.; Zhou, H.; Huang, B.; Yao, G.; Lai, B. Critical review of natural iron-based minerals used as heterogeneous catalysts in peroxide activation processes: Characteristics, applications and mechanisms. *J. Hazard. Mater.* **2021**, *416*, 125809.
14. Teel, A.L.; Ahmad, M.; Watts, R.J. Persulfate activation by naturally occurring trace minerals. *J. Hazard. Mater.* **2011**, *196*, 153–159.
15. Wang, J.; Wang, S. Activation of persulfate (PS) and peroxymonosulfate (PMS) and application for the degradation of emerging contaminants. *Chem. Eng. J.* **2018**, *334*, 1502–1517.
16. Zhang, L.S.; Jiang, X.H.; Zhong, Z.A.; Tian, L.; Sun, Q.; Cui, Y.T.; Lu, X.; Zou, J.P.; Luo, S.L. Carbon nitride supported high-loading Fe single-atom catalyst for activation of peroxymonosulfate to generate $^1O_2$ with 100% selectivity. *Angew. Chem. Int. Ed.* **2021**, *60*, 21751–21755.
17. Wu, J.; Wang, B.; Cagnetta, G.; Huang, J.; Wang, Y.; Deng, S.; Yu, G. Nanoscale zero valent iron-activated persulfate coupled with Fenton oxidation process for typical pharmaceuticals and personal care products degradation. *Sep. Purif. Technol.* **2020**, *239*, 116534.
18. Zhong, J.; Feng, Y.; Li, J.-L.; Yang, B.; Ying, G.-G. Removal of sulfadiazine using 3D interconnected petal-like magnetic reduced graphene oxide (MrGO) nanocomposites. *Water* **2020**, *12*, 1933.
19. Ding, Y.; Wang, X.; Fu, L.; Peng, X.; Pan, C.; Mao, Q.; Wang, C.; Yan, J. Nonradicals induced degradation of organic pollutants by peroxydisulfate (PDS) and peroxymonosulfate (PMS): Recent advances and perspective. *Sci. Total Environ.* **2020**, *765*, 142794.
20. Gao, Y.; Chen, Z.; Zhu, Y.; Li, T.; Hu, C. New insights into the generation of singlet oxygen in the metal-free peroxymonosulfate activation process: Important role of electron-deficient carbon atoms. *Environ. Sci. Technol.* **2020**, *54*, 1232.
21. Sun, W.; Pang, K.; Ye, F.; Pu, M.; Zhou, C.; Huang, H.; Zhang, Q.; Niu, J. Carbonization of camphor sulfonic acid and melamine to N,S-co-doped carbon for sulfamethoxazole degradation via persulfate activation: Nonradical dominant pathway. *Sep. Purif. Technol.* **2021**, *279*, 119723.
22. Ali, I.; Basheer, A.A.; Kucherova, A.; Memetov, N.; Pasko, T.; Ovchinnikov, K.; Pershin, V.; Kuznetsov, D.; Galunin, E.; Grachev, V.; Tkachev, A. Advances in carbon nanomaterials as lubricants modifiers. *J. Mol. Liq.* **2019**, *279*, 251–266.
23. Al-Shaalan, N.H.; Ali, I.; Alothman, Z.A.; Al-Wahaibi, L.H.; Alabdulmonem, H. High performance removal and simulation studies of diuron pesticide in water on MWCNTs. *J. Mol. Liq.* **2019**, *289*, 111039.
24. Ali, I.; Babkin, A.V.; Burakova, I.V.; Burakov, A.E.; Neskoromnaya, E.A.; Tkachev, A.G.; Panglisch, S.; AlMasoud, N.; Alomar, T.S. Fast removal of samarium ions in water on highly efficient nanocomposite based graphene oxide modified with polyhydroquinone: Isotherms, kinetics, thermodynamics and desorption. *J. Mol. Liq.* **2021**, *329*, 115584.
25. Feng, Y.; Li, H.L.; Lin, L.; Kong, L.J.; Li, X.Y.; Wu, D.L.; Zhao, H.Y.; Shih, K. Degradation of 1,4-dioxane via controlled generation of radicals by pyrite-activated oxidants: Synergistic effects, role of disulfides, and activation sites. *Chem. Eng. J.* **2018**, *336*, 416–426.

26. Li, Y.; Chen, J.; Zhong, J.; Yang, B.; Yang, Z.; Shih, K.; Feng, Y. Acceleration of traces of Fe^{3+}-activated peroxymonosulfate by natural pyrite: A novel cocatalyst for improving Fenton-like processes. *Chem. Eng. J.* **2022**, *435*, 134893.
27. Li, T.; Abdelhaleem, A.; Chu, W.; Xu, W. Efficient activation of oxone by pyrite for the degradation of propanil: Kinetics and degradation pathway. *J. Hazard. Mater.* **2021**, *403*, 123930.
28. Zhou, Y.; Wang, X.; Zhu, C.; Dionysiou, D.D.; Zhao, G.; Fang, G.; Zhou, D. New insight into the mechanism of peroxymonosulfate activation by sulfur-containing minerals: Role of sulfur conversion in sulfate radical generation. *Water Res.* **2018**, *142*, 208–216.
29. Xiang, W.; Chen, H.; Zhong, Z.; Zhang, C.; Lu, X.; Huang, M.; Zhou, T.; Yu, P.; Zhang, B. Efficient degradation of carbamazepine in a neutral sonochemical FeS/persulfate system based on the enhanced heterogeneous-homogeneous sulfur-iron cycle. *Sep. Purif. Technol.* **2022**, *282*, 120041.
30. Feng, Y.; Wu, D.; Deng, Y.; Zhang, T.; Shih, K. Sulfate radical-mediated degradation of sulfadiazine by $CuFeO_2$ rhombohedral crystal-catalyzed peroxymonosulfate: Synergistic effects and mechanisms. *Environ. Sci. Technol.* **2016**, *50*, 3119–3127.
31. Huang, G.X.; Wang, C.Y.; Yang, C.W.; Guo, P.C.; Yu, H.Q. Degradation of bisphenol A by peroxymonosulfate catalytically activated with $Mn_{1.8}Fe_{1.2}O_4$ nanospheres: Synergism between Mn and Fe. *Environ. Sci. Technol.* **2017**, *51*, 12611–12618.
32. Yao, J.; Zeng, X.; Wang, Z. Enhanced degradation performance of sulfisoxazole using peroxymonosulfate activated by copper-cobalt oxides in aqueous solution: Kinetic study and products identification. *Chem. Eng. J.* **2017**, *330*, 345–354.
33. Dong, H.; Yuan, X.; Wang, W.; Qiang, Z. Occurrence and removal of antibiotics in ecological and conventional wastewater treatment processes: A field study. *J. Environ. Manag.* **2016**, *178*, 11–19.
34. Liu, X.; Steele, J.C.; Meng, X.-Z. Usage, residue, and human health risk of antibiotics in Chinese aquaculture: A review. *Environ. Pollut.* **2017**, *223*, 161–169.
35. Antonijević, M.M.; Janković, Z.D.; Dimitrijević, M.D. Kinetics of chalcopyrite dissolution by hydrogen peroxide in sulphuric acid. *Hydrometallurgy* **2004**, *71*, 329–334.
36. Liang, C.; Huang, C.; Mohanty, N.; Kurakalva, R.M. A rapid spectrophotometric determination of persulfate anion in ISCO. *Chemosphere* **2008**, *73*, 1540–1543.
37. Yin, R.; Guo, W.; Wang, H.; Du, J.; Zhou, X.; Wu, Q.; Zheng, H.; Chang, J.; Ren, N. Selective degradation of sulfonamide antibiotics by peroxymonosulfate alone: Direct oxidation and nonradical mechanisms. *Chem. Eng. J.* **2018**, *334*, 2539–2546.
38. Ji, Y.; Lu, J.; Wang, L.; Jiang, M.; Yang, Y.; Yang, P.; Zhou, L.; Ferronato, C.; Chovelon, J.-M. Non-activated peroxymonosulfate oxidation of sulfonamide antibiotics in water: Kinetics, mechanisms, and implications for water treatment. *Water Res.* **2018**, *147*, 82–90.
39. Ghanbari, F.; Moradi, M. Application of peroxymonosulfate and its activation methods for degradation of environmental organic pollutants: Review. *Chem. Eng. J.* **2017**, *310*, 41.
40. Peng, J.; Zhou, H.; Liu, W.; Ao, Z.; Ji, H.; Liu, Y.; Su, S.; Yao, G.; Lai, B. Insights into heterogeneous catalytic activation of peroxymonosulfate by natural chalcopyrite: pH-dependent radical generation, degradation pathway and mechanism. *Chem. Eng. J.* **2020**, *397*, 125387.
41. Boreen, A.L.; Arnold, W.A.; McNeill, K. Photochemical fate of sulfa drugs in the aquatic environment: Sulfa drugs containing five-membered heterocyclic groups. *Environ. Sci. Technol.* **2004**, *38*, 3933–3940.
42. Wang, Z.; Wang, Z.; Li, W.; Lan, Y.; Chen, C. Performance comparison and mechanism investigation of Co_3O_4-modified different crystallographic MnO_2 (α, β, γ, and δ) as an activator of peroxymonosulfate (PMS) for sulfisoxazole degradation. *Chem. Eng. J.* **2022**, *427*, 130888.
43. Davies, M.J.; Gilbert, B.C.; Stell, J.K.; Whitwood, A.C. Nucleophilic substitution reactions of spin adducts. Implications for the correct identification of reaction intermediates by EPR/spin trapping. *J. Chem. Soc. Perkin Trans. 2* **1992**, 333–335. https://pubs.rsc.org/en/content/articlelanding/1992/P2/p29920000333 (accessed on 28 October 2022)
44. Timmins, G.S.; Liu, K.J.; Bechara, E.J.; Kotake, Y.; Swartz, H.M. Trapping of free radicals with direct in vivo EPR detection: A comparison of 5, 5-dimethyl-1-pyrroline-N-oxide and 5-diethoxyphosphoryl-5-methyl-1-pyrroline-N-oxide as spin traps for HO and SO4•⁻. *Free Radic. Biol. Med.* **1999**, *27*, 329–333.
45. McElroy, W.; Waygood, S. Kinetics of the reactions of the SO_4^- radical with SO_4^{-}, $S_2O_8^{2-}$, H_2O and Fe^{2+}, Journal of the Chemical Society. *Faraday Trans.* **1990**, *86*, 2557–2564.
46. Ross, A.B.; Neta, P. *Rate Constants for Reactions of Inorganic Radicals in Aqueous Solution*; US Department of Commerce, National Bureau of Standards: Washington, WA, USA, 1979.
47. Clifton, C.L.; Huie, R.E. Rate constants for hydrogen abstraction reactions of the sulfate radical, SO_4^-. Alcohols. *Int. J. Chem. Kinet.* **1989**, *21*, 677–687.
48. Buxton, G.V.; Greenstock, C.L.; Helman, W.P.; Ross, A.B. Critical review of rate constants for reactions of hydrated electrons, hydrogen atoms and hydroxyl radicals (·OH/·O^-) in aqueous solution. *J. Phys. Chem. Ref. Data* **1988**, *17*, 513–886.
49. Eibenberger, H.; Steenken, S.; O'Neill, P.; Schulte-Frohlinde, D. Pulse radiolysis and electron spin resonance studies concerning the reaction of SO_4.cntdot.- with alcohols and ethers in aqueous solution. *J. Phys. Chem.* **1978**, *82*, 749–750.
50. Zhou, R.; Liu, S.; He, F.; Ren, H.; Han, Z. Alkylpolyglycoside modified $MnFe_2O_4$ with abundant oxygen vacancies boosting singlet oxygen dominated peroxymonosulfate activation for organic pollutants degradation. *Chemosphere* **2021**, *285*, 131433.

51. Wang, L.; Xu, H.; Jiang, N.; Wang, Z.; Jiang, J.; Zhang, T. Trace cupric species triggered decomposition of peroxymonosulfate and degradation of organic pollutants: Cu(III) being the primary and selective intermediate oxidant. *Environ. Sci. Technol.* **2020**, *54*, 4686.
52. Chen, J.; Zhou, X.; Sun, P.; Zhang, Y.; Huang, C.H. Complexation enhances Cu(II)-activated peroxydisulfate: A novel activation mechanism and Cu(III) contribution. *Environ. Sci. Technol.* **2019**, *53*, 11774–11782.
53. Zong, Y.; Guan, X.; Xu, J.; Feng, Y.; Mao, Y.; Xu, L.; Chu, H.; Wu, D. Unraveling the overlooked involvement of high-valent cobalt-oxo species generated from the cobalt(II)-activated peroxymonosulfate process. *Environ. Sci. Technol.* **2020**, *54*, 16231–16239.
54. Haag, W.R.; Hoigne, J. Singlet oxygen in surface waters. 3. Photochemical formation and steady-state concentrations in various types of waters. *Environ. Sci. Technol.* **1986**, *20*, 341.
55. Feng, Y.; Qing, W.; Kong, L.; Li, H.; Wu, D.; Fan, Y.; Lee, P.H.; Shih, K. Factors and mechanisms that influence the reactivity of trivalent copper: A novel oxidant for selective degradation of antibiotics. *Water Res.* **2019**, *149*, 1–8.
56. Wang, Y.; Wu, Y.; Yu, Y.; Pan, T.; Li, D.; Lambropoulou, D.; Yang, X. Natural polyphenols enhanced the Cu(II)/peroxymonosulfate (PMS) oxidation: The contribution of Cu(III) and HO•. *Water Res.* **2020**, *186*, 116326.
57. Ding, Y.; Zhu, L.; Wang, N.; Tang, H. Sulfate radicals induced degradation of tetrabromobisphenol A with nanoscaled magnetic $CuFe_2O_4$ as a heterogeneous catalyst of peroxymonosulfate. *Appl. Catal. B* **2013**, *129*, 153–162.
58. Feng, Y.; Lee, P.H.; Wu, D.; Zhou, Z.; Li, H.; Shih, K. Degradation of contaminants by Cu^{+}-activated molecular oxygen in aqueous solutions: Evidence for cupryl species (Cu^{3+}). *J. Hazard. Mater.* **2017**, *331*, 81–87.
59. Pérez-Almeida, N.; González-Dávila, M.; Santana-Casiano, J.M.; González, A.G.; de Tangil, M.S. Oxidation of Cu(I) in seawater at low oxygen concentrations. *Environ. Sci. Technol.* **2013**, *47*, 1239–1247.
60. Wang, H.; Liao, B.; Hu, M.; Ai, Y.; Wen, L.; Yang, S.; Ye, Z.; Qin, J.; Liu, G. Heterogeneous activation of peroxymonosulfate by natural chalcopyrite for efficient remediation of groundwater polluted by aged landfill leachate. *Appl. Catal. B* **2022**, *300*, 120744.
61. Jayson, G.G.; Parsons, B.J.; Swallow, A.J. Some simple, highly reactive, inorganic chlorine derivatives in aqueous solution. Their formation using pulses of radiation and their role in the mechanism of the Fricke dosimeter. *J. Chem. Soc. Faraday Trans. 1* **1973**, *69*, 1597–1607.
62. Lente, G.; Kalmár, J.; Baranyai, Z.; Kun, A.; Kék, I.; Bajusz, D.; Takács, M.; Veres, L.; Fábián, I. One-versus two-electron oxidation with peroxomonosulfate ion: Reactions with iron(II), vanadium(IV), halide ions, and photoreaction with cerium(III). *Inorg. Chem.* **2009**, *48*, 1763–1773.
63. Grebel, J.E.; Pignatello, J.J.; Mitch, W.A. Effect of halide ions and carbonates on organic contaminant degradation by hydroxyl radical-based advanced oxidation processes in saline waters. *Environ. Sci. Technol.* **2010**, *44*, 6822–6828.
64. Lei, X.; Lei, Y.; Guan, J.; Westerhoff, P.; Yang, X. Kinetics and transformations of diverse dissolved organic matter fractions with sulfate radicals. *Environ. Sci. Technol.* **2022**, *56*, 4457–4466.
65. Chen, J.; Gu, B.; Royer, R.A.; Burgos, W.D. The roles of natural organic matter in chemical and microbial reduction of ferric iron. *Sci. Total Environ.* **2003**, *307*, 167–178.
66. Ye, Q.; Wu, J.; Wu, P.; Wang, J.; Niu, W.; Yang, S.; Chen, M.; Rehman, S.; Zhu, N. Enhancing peroxymonosulfate activation of Fe-Al layered double hydroxide by dissolved organic matter: Performance and mechanism. *Water Res.* **2020**, *185*, 116246.
67. Zhou, Y.; Jiang, J.; Gao, Y.; Ma, J.; Pang, S.Y.; Li, J.; Lu, X.T.; Yuan, L.P. Activation of peroxymonosulfate by benzoquinone: A novel nonradical oxidation process. *Environ. Sci. Technol.* **2015**, *49*, 12941–12950.